Prompt charmonia production and polarization at the LHC in the NRQCD with k_T-factorization. III. J/ψ meson

S. P. Baranov[1] and A. V. Lipatov[2,3]

[1]*P.N. Lebedev Physics Institute, 119991 Moscow, Russia*
[2]*Skobeltsyn Institute of Nuclear Physics, Lomonosov Moscow State University, 119991 Moscow, Russia*
[3]*Joint Institute for Nuclear Research, Dubna 141980, Moscow region, Russia*

In the framework of the k_T-factorization approach, the production and polarization of prompt J/ψ mesons at the LHC energies is studied. Our consideration is based on the nonrelativistic QCD formalism for bound states and off-shell amplitudes for hard partonic subprocesses. Both the direct production mechanism and feed-down contributions from χ_c and $\psi(2S)$ decays are taken into account. The transverse momentum dependent (or unintegrated) gluon densities in a proton were derived from Ciafaloni-Catani-Fiorani-Marchesini evolution equation or, alternatively, were chosen in accordance with Kimber-Martin-Ryskin prescription. The nonperturbative color-octet matrix elements were first deduced from the fits to the latest CMS data on J/ψ transverse momentum distributions and then applied to describe the ATLAS and LHCb data on J/ψ production and polarization at $\sqrt{s} = 7$, 8 and 13 TeV. We perform an estimation of polarization parameters λ_θ, λ_ϕ, and $\lambda_{\theta\phi}$ which determine J/ψ spin density matrix and demonstrate that treating the soft gluon emission as a series of explicit color-electric dipole transitions within NRQCD leads to unpolarized J/ψ production at high transverse momenta, that is in qualitative agreement with the LHC data.

I. INTRODUCTION

Since it was first observed, inclusive J/ψ meson production in hadronic collisions is a subject of considerable theoretical and experimental interest. It serves as a complex probe of the hadron structure, perturbative QCD and the formation mechanism of charmed quark bound states. Indeed, the production of unbound $c\bar{c}$ pairs in hard scattering (described by perturbative QCD) is followed by the formation of bound states that is essentially a nonperturbative process. The latter seems to be the most tricky ingredient in the theory.

Two theoretical approaches describing this nonperturbative step are known in the literature under the names of color-singlet (CS) [1] and color-octet(CO) [2] models. In general, the charmed quark pair is produced in a state $^{2S+1}L_J^{(a)}$ with spin S, orbital angular momentum L, total angular momentum J and color a, which can be either identical to the final charmonium quantum numbers (as accepted in the CS model) or different from those. In the latter case, the produced $c\bar{c}$ pair transforms into physical charmonium state by means of soft (nonperturbative) gluon radiation, as considered in the formalism of nonrelativistic QCD (NRQCD) [3,4]. The probability to form a given bound state is determined by the respective nonperturbative long-distance matrix elements (NMEs), which are assumed to be universal (process-independent), not depending on the charmonium momentum and obeying certain hierarchy in powers of the relative charmed quarks velocity v.

As we have explained in our previous papers [5,6], none of the existing theoretical approaches is able to describe all of the data in their integrity. The CS predictions obtained at the dominant tree-level next-to-next-to-leading order (NNLO*) [7,8] underestimate the measured J/ψ and $\psi(2S)$ cross sections by a factor of 5, that is well off the theoretical and experimental uncertainty band [9]. In the NRQCD formalism, a reasonably good description of the transverse momentum distributions can be achieved at the next-to-leading order (NLO) by adjusting the NMEs values, which play the role of free parameters [10–15]. However, these NMEs dramatically depend on the minimal charmonium transverse momentum used in the fits [16] and are incompatible with each other (both in size and even in sign) when obtained from fitting the different data sets. Moreover, the worst problem of the calculations is connected with J/ψ spin alignment. If, as predicted, the dominant contribution comes from the gluon fragmentation into an octet $c\bar{c}$ pair, the outgoing J/ψ must have strong transverse polarization. The latter disagrees with the Tevatron [17,18] and LHC measurements [19–21] which point to unpolarized or even longitudinally polarized particles. The overall situation is known as "quarkonium polarization puzzle" and understood as a deep crisis.

Recently, a new solution to this polarization puzzle has been proposed [22] in the framework of a model that interprets the soft final state gluon radiation (transforming an unbound $c\bar{c}$ pair into physical charmonium state) as a series of color-electric dipole transitions. In contrast with

the usual NRQCD calculations where the emitted gluons are not presented explicitly in the final state, it was proposed to represent the long-distance NMEs in an explicit form inspired by classical multipole radiation theory, so that the spin structure of the transition amplitudes is specified. This model differs in its predictions from the conventional LO and NLO calculations (both CS and CO), as the final-state soft gluons are now emitted by the entire $c\bar{c}$ system and not by individual quarks. This scenario results in the unpolarized (or only weakly polarized) heavy quarkonia, providing us with an easy and natural solution of the long-standing puzzle. Moreover, it was already successfully applied [5] to describe the recent LHC data on the production and polarization of $\psi(2S)$ mesons.

In the present paper we consider the production and polarization of J/ψ mesons at the LHC conditions using the approach [22]. This study is a continuation of the works [5,6], where the $\psi(2S)$ and χ_c meson production at the LHC has been considered. We give a systematic analysis of ATLAS [23], CMS [21,24], and LHCb [20,25,26] data collected at $\sqrt{s} = 7$, 8 and 13 TeV regarding the transverse momentum distributions and polarization parameters λ_θ, λ_ϕ, and $\lambda_{\theta\phi}$ which determine the spin density matrix of the produced J/ψ mesons. To describe the perturbative production of $c\bar{c}$ pair in a short-distance gluon-gluon fusion subprocess we employ the k_T-factorization approach [27,28]. The latter is based on the Balitsky-Fadin-Kuraev-Lipatov (BFKL) [29] or Ciafaloni-Catani-Fiorani-Marchesini (CCFM) [30] gluon evolution equations. We see certain advantages in the fact that, even with the leading-order (LO) partonic amplitudes, one then includes a large piece of high-order corrections (namely, part of NLO + NNLO + ... terms containing the leading logarithms of the type $\log 1/x$ due to real parton emissions in initial state) taking them into account in the form of transverse momentum dependent (TMD) parton densities.[1] Besides that, the latter absorb the effects of soft gluon resummation, that regularizes the infrared divergences and makes our predictions applicable even at low transverse momenta. Two sources of J/ψ production are taken into account: direct J/ψ production and feed-down from radiative decays of heavier charmonium states like χ_{c1}, χ_{c2} or $\psi(2S)$, that is in full agreement with the experimental setup [20,21,23–26]. In the literature, these two joint sources are referred to as prompt J/ψ production.[2]

The outline of our paper is the following. In Sec. II we briefly recall the NRQCD formalism and the k_T-factorization approach. In Sec. III we perform a numerical fit to the latest CMS data and extract the color-octet

NMEs for J/ψ mesons using three different sets of TMD gluon distributions. Later in this section we check the compatibility of the extracted parameters with ATLAS and LHCb data on J/ψ production and polarization. The comparison is followed by a discussion. Our conclusions are collected in Sec. IV.

II. THEORETICAL FRAMEWORK

The details of calculations can be found in our previous papers [5,6]. Here we briefly recall the most important steps only. Our consideration is based on the following leading-order off-shell gluon-gluon fusion subprocesses:

$$g^*(k_1) + g^*(k_2) \to c\bar{c}[^3S_1^{(1)}](p) + g(k), \quad (1)$$

$$g^*(k_1) + g^*(k_2) \to c\bar{c}[^1S_0^{(8)}, {}^3S_1^{(8)}, {}^3P_J^{(8)}](p), \quad (2)$$

for S-wave charmonia, i.e., J/ψ or $\psi(2S)$ mesons, followed by nonperturbative transitions $c\bar{c} \to J/\psi, \psi(2S) + X$, and

$$g^*(k_1) + g^*(k_2) \to c\bar{c}[^3P_J^{(1)}, {}^3S_1^{(8)}](p), \quad (3)$$

followed by nonperturbative transitions $c\bar{c} \to \chi_{cJ} + X$ for P-wave states, where $J = 0$, 1 or 2 and the four-momenta of all particles are indicated in the parentheses. The corresponding production amplitudes can be obtained from the one for an unspecified $c\bar{c}$ state by applying the appropriate projection operators, which guarantee the proper quantum numbers of the $c\bar{c}$ state under consideration. For the different spin and orbital angular momentum states these operators read [1]:

$$\Pi[^1S_0] = \gamma_5(\hat{p}_c + m_c)/m^{1/2}, \quad (4)$$

$$\Pi[^3S_1] = \hat{\epsilon}(S_z)(\hat{p}_c + m_c)/m^{1/2}, \quad (5)$$

$$\Pi[^3P_J] = (\hat{p}_{\bar{c}} - m_c)\hat{\epsilon}(S_z)(\hat{p}_c + m_c)/m^{3/2}, \quad (6)$$

where $m = 2m_c$ is the mass of the considered $c\bar{c}$ state, p_c and $p_{\bar{c}}$ are the four-momenta of the charmed quark and antiquark, $p_c = p/2 + q$, $p_{\bar{c}} = p/2 - q$, and q is the relative four-momentum of the quarks in the bound state. In accordance with the nonrelativistic bound state formalism, the charmed quark mass m_c is always set equal to $1/2$ of the charmonium mass. States with various projections of the spin momentum onto the z axis are represented by the polarization four-vector $\epsilon_\mu(S_z)$.

The probability for the charmed quarks to form a meson depends on the real (for color singlets) or fictitious (for color octets) bound state wave functions $\Psi^{(a)}(q)$, so that one has to multiply the hard subprocess amplitude $\mathcal{A}$ (depending on q) by the meson wave function $\Psi^{(a)}(q)$ and integrate over q. The integration is done after expanding the amplitude $\mathcal{A}$ around $q = 0$ and keeping the leading

---

[1]A detailed description of the k_T-factorization approach can be found, for example, in reviews [31].

[2]In pp collisions, J/ψ mesons can be also produced via decays of b-flavored hadrons. This process which is usually referred to as nonprompt J/ψ production or "J/ψ-from-b" is out of our present consideration.

terms only. The corresponding NMEs are related to the wave functions in the coordinate space $\mathcal{R}^{(a)}(x)$, which are the Fourier transforms of $\Psi^{(a)}(q)$ and their derivatives [2–4]:

$$\langle \mathcal{O}[^{2S+1}L_J^{(a)}] \rangle = 2N_c(2J+1)|\mathcal{R}^{(a)}(0)|^2/4\pi, \quad (7)$$

for S-waves and

$$\langle \mathcal{O}[^{2S+1}L_J^{(a)}] \rangle = 6N_c(2J+1)|\mathcal{R}'^{(a)}(0)|^2/4\pi, \quad (8)$$

for P-waves. The CS wave functions at the origin of coordinate space for J/ψ and $\psi(2S)$ states are known from their measured leptonic decay width. The CS wave functions of χ_{cJ} states are taken from our previous paper [6]. The color-octet NMEs are not calculable within the theory and can only be extracted from fits to experimental data. For more details the reader can address the original papers [1–4] or our previous notes [5,6]. After squaring and summation over polarizations, our analytical expressions for all perturbative amplitudes agree with the ones presented in [32].

An important point in the NRQCD formalism is the emission of soft gluons after the hard interaction. As it was already mentioned above, it is usually assumed that the emitted soft gluons bring away the unwanted color and change other quantum numbers of the $c\bar{c}$ system but do not carry any energy, thus keeping the kinematics intact. However, this is in obvious contradiction with confinement which prohibits the emission of infinitely soft colored quanta. In order that the quantum numbers get changed, one needs to radiate a real gluon with some energy $E \sim \Lambda_{\mathrm{QCD}}$, giving us the confidence that we do not enter into the confinement or perturbative domains [33]. This issue is not the matter of only kinematic corrections, because we cannot organize a transition amplitude with correct spin properties without having a nonzero energy-momentum transfer. Following [22], we describe this step in terms of electric dipole ($E1$) transitions that dominate the multipole expansion. In the case of $^3P_J^{(8)}$ states, a single $E1$ transition is needed to transform them into $^3S_1$ mesons. The corresponding amplitudes can be written as [34]:

$$\mathcal{A}(^3P_0^{(8)} \to \psi + g) \sim k_\mu^{(g)} p^{(\mathrm{CO})\mu} \epsilon_\nu^{(\psi)} \epsilon^{(g)\nu}, \quad (9)$$

$$\mathcal{A}(^3P_1^{(8)} \to \psi + g) \sim e^{\mu\nu\alpha\beta} k_\mu^{(g)} \epsilon_\nu^{(\mathrm{CO})} \epsilon_\alpha^{(\psi)} \epsilon_\beta^{(g)}, \quad (10)$$

$$\mathcal{A}(^3P_2^{(8)} \to \psi + g) \sim p^{(\mathrm{CO})\mu} \epsilon^{(\mathrm{CO})\alpha\beta} \epsilon_\alpha^{(\psi)} [k_\mu^{(g)} \epsilon_\beta^{(g)} - k_\beta^{(g)} \epsilon_\mu^{(g)}], \quad (11)$$

where $p_\mu^{(\mathrm{CO})}$, $k_\mu^{(g)}$, $\epsilon_\mu^{(\psi)}$, $\epsilon_\mu^{(g)}$, $\epsilon_\mu^{(\mathrm{CO})}$, and $\epsilon_{\mu\nu}^{(\mathrm{CO})}$ are the four-momenta and polarization four-vectors (tensor) of the respective particles, and $e^{\mu\nu\alpha\beta}$ is the fully antisymmetric

Levi-Civita tensor. These amplitudes are practically the same as the ones for radiative decays of χ_c mesons, the only difference is in the overall normalization factors. In the case of $^3S_1^{(8)}$ state, we treat its transformation into real $^3S_1$ meson as two successive color-electric dipole transitions, $^3S_1^{(8)} \to {}^3P_J^{(8)} + g$, $^3P_J^{(8)} \to \psi + g$, proceeding via either of the three intermediate $^3P_J^{(8)}$ states, where $J = 0$, 1 or 2, and exploit the same effective coupling vertices (9)—(11). Now, the polarization of the outgoing mesons can also be calculated without any ambiguity. Below we use the expressions derived in our previous papers [5,6].

The integral production cross section is calculated in the k_T-factorization approach as a convolution of the off-shell partonic cross sections and the TMD gluon densities in a proton. The contribution from the CS mechanism can be presented as

$$\sigma(pp \to \psi + X)$$
$$= \int \frac{1}{16\pi(x_1 x_2 s)^2} f_g(x_1, \mathbf{k}_{1T}^2, \mu^2) f_g(x_2, \mathbf{k}_{2T}^2, \mu^2)$$
$$\times |\bar{\mathcal{A}}(g^* + g^* \to \psi + g)|^2 d\mathbf{p}_T^2 d\mathbf{k}_{1T}^2 d\mathbf{k}_{2T}^2 dy dy_g \frac{d\phi_1}{2\pi} \frac{d\phi_2}{2\pi}, \quad (12)$$

where $f_g(x, \mathbf{k}_T^2, \mu^2)$ is the TMD gluon density, $\mathbf{p}_T$ and y are the transverse momentum and rapidity of produced J/ψ meson, y_g is the rapidity of outgoing gluon, and $\sqrt{s}$ is the pp center-of-mass energy. The initial off-shell gluons have the fractions x_1 and x_2 of the parent protons longitudinal momenta, nonzero transverse momenta $\mathbf{k}_{1T}$ and $\mathbf{k}_{2T}$ ($\mathbf{k}_{1T}^2 = -k_{1T}^2 \neq 0$, $\mathbf{k}_{2T}^2 = -k_{2T}^2 \neq 0$) and azimuthal angles ϕ_1 and ϕ_2. For the CO production we have:

$$\sigma(pp \to \psi + X)$$
$$= \int \frac{2\pi}{x_1 x_2 s F} f_g(x_1, \mathbf{k}_{1T}^2, \mu^2) f_g(x_2, \mathbf{k}_{2T}^2, \mu^2)$$
$$\times |\bar{\mathcal{A}}(g^* + g^* \to \psi)|^2 d\mathbf{k}_{1T}^2 d\mathbf{k}_{2T}^2 dy \frac{d\phi_1}{2\pi} \frac{d\phi_2}{2\pi}. \quad (13)$$

According to the general definition [35], the off-shell gluon flux factor in (13) is defined[3] as $F = 2\lambda^{1/2}(\hat{s}, k_1^2, k_2^2)$, where $\hat{s} = (k_1 + k_2)^2$. Everywhere, the multidimensional integration has been performed by means of the Monte Carlo technique, using the routine VEGAS [37].

As we did in our previous papers [5,6], we tried numerically several sets of TMD gluon densities in a proton. Two of them (A0 [38] and JH'2013 [39]) were obtained from CCFM equation where all input parameters were fitted to the proton structure function $F_2(x, Q^2)$.

---

[3]The dependence of numerical predictions on the different forms of flux factor has been studied in [36].

Besides that, we used a parametrization obtained with Kimber-Martin-Ryskin (KMR) prescription [40] which provides a method to construct the TMD quark and gluon densities out of conventional (collinear) distributions. In that case, we used for the input the leading-order Martin-Stirling-Thorn-Watt (MSTW'2008) set [41].

III. NUMERICAL RESULTS

We are now in a position to present our numerical results. First we describe our input and kinematic conditions. Having the TMD gluon densities chosen, the cross sections (12) and (13) depend on the renormalization and factorization scales μ_R and μ_F. We set $\mu_R^2 = m^2 + \mathbf{p}_T^2$ and $\mu_F^2 = \hat{s} + \mathbf{Q}_T^2$, where $\mathbf{Q}_T$ is the transverse momentum of the initial off-shell gluon pair. The choice of μ_R is the standard one for studying the charmonia production, whereas the special choice of μ_F is connected with the CCFM evolution [38,39]. Following [42], we set J/ψ mass $m = 3.0969$ GeV, branching fraction $B(J/\psi \to l^+ l^-) = 0.05961$ and use the LO formula for the coupling constant $\alpha_s(\mu^2)$ with $n_f = 4$ quark flavors and $\Lambda_{\text{QCD}} = 200$ MeV, so that $\alpha_s(M_Z^2) = 0.1232$. When calculating the feed-down contributions from radiative decays of χ_c and $\psi(2S)$ mesons, we used exactly the same parameters and NMEs as in our previous papers [5,6].

First, we determine the whole set of J/ψ meson NMEs. We have fitted the transverse momentum distributions of J/ψ mesons measured recently by the CMS Collaboration at $\sqrt{s} = 7$ TeV [24]. These measurements were done at central rapidities $|y| < 1.2$ and moderate and high transverse momenta $10 < p_T < 100$ GeV, where the NRQCD formalism is believed to be most reliable. We performed the fitting procedure under requirement that the NMEs be strictly positive. Further on, instead of taking the color singlet NME from the $J/\psi \to l^+ l^-$ partial decay width, we treat it as free parameter. A comparison of such fitted NME with the ones known from leptonic decay will provide an independent cross-check of our calculations and an additional test for the TMD gluon densities in a proton.

In Table I we list our results for the NMEs fits obtained for three different TMD gluon distributions. For comparison, we also present here two sets of NMEs [11,15], obtained within the NLO NRQCD by other authors. The

main difference between them is in that these fits were based on differently selected data sets. One can see that our fitting procedure leads to very similar values of the CS NME extracted with the considered TMD gluon densities. On the contrary, the fitted CO NME values strongly depend on the choice of TMD gluon distribution. Typically, they are smaller than the ones obtained in the NLO NRQCD fits [11,15], that is almost consistent with the estimates performed by other authors [43,44]. We find that the $^3P_J^{(8)}$ contributions are compatible with zero, that agrees with the early consideration [32]. Note that, as it was expected, our fitted CS MNEs are close to the ones determined from the $J/\psi \to l^+ l^-$ decay, $\langle \mathcal{O}^\psi [^3S_1^{(1)}] \rangle \sim$ 1.3–1.5 GeV^3, that demonstrates self-consistency of our calculations and good agreement with the previous ones [45], which were performed in the CS model alone at relatively low transverse momenta $p_T < 30$ GeV.

Now we turn to comparing our predictions with the latest data collected by the ATLAS [23], CMS [21,24], and LHCb [20,25,26] Collaborations. Recently, the ATLAS Collaboration presented prompt J/ψ transverse momentum distributions at $8 < p_T < 100$ GeV and $\sqrt{s} = 7$ TeV and $8 < p_T < 110$ GeV and $\sqrt{s} = 8$ TeV for eight subdivisions in J/ψ rapidity y. The CMS Collaboration measured J/ψ transverse momentum spectra in the kinematic range $10 < p_T < 100$ GeV and $|y| < 1.2$, and the LHCb Collaboration measured them in the range $p_T < 14$ GeV and $2 < y < 4.5$ at different energies $\sqrt{s} = 7$, 8 and 13 TeV. Our predictions for the differential cross sections are presented in Figs. 1–3 in comparison with the LHC data. As usual, to estimate the theoretical uncertainty of our calculations coming from the hard scales, we vary them by a factor of 2 around the default values. One can see that at central rapidities we achieved a reasonably good agreement between our calculations (with any of the considered TMD gluon densities) and CMS and ATLAS data in the whole p_T region within the uncertainties. However, with increasing rapidity, the overall description of ATLAS data becomes a bit worse: our central predictions tend to slightly underestimate the data at low and moderate p_T (see Fig. 2). We note that the observed discrepancy is not catastrophic, because some reasonable variation in the factorization and/or renormalization scales (shown by the shaded bands)

TABLE I.　The NMEs for J/ψ meson derived from the fit of the CMS data [24]. The NMEs obtained in the NLO NRQCD fits [11,15] are shown for comparison.

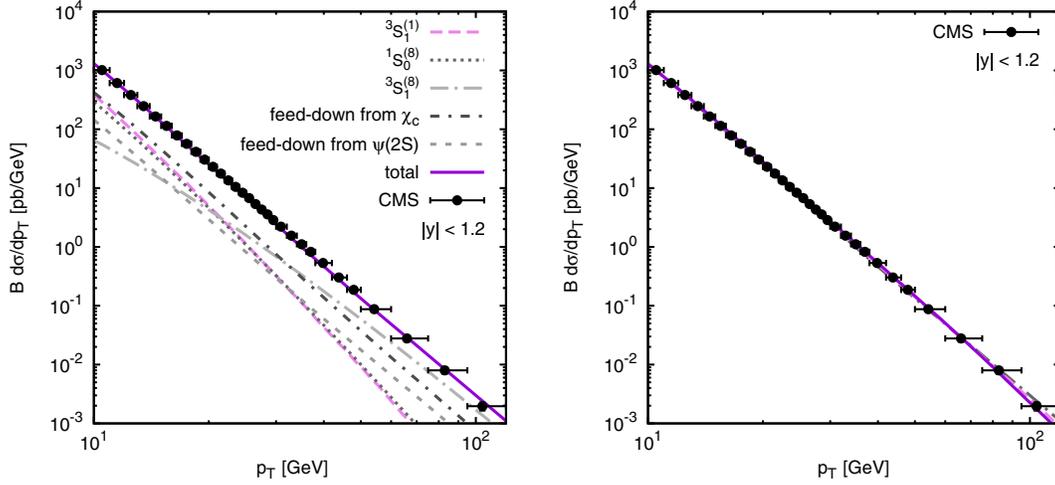|	$\langle \mathcal{O}^\psi [^3S_1^{(1)}] \rangle / \text{GeV}^3$	$\langle \mathcal{O}^\psi [^1S_0^{(8)}] \rangle / \text{GeV}^3$	$\langle \mathcal{O}^\psi [^3S_1^{(8)}] \rangle / \text{GeV}^3$	$\langle \mathcal{O}^\psi [^3P_0^{(8)}] \rangle / \text{GeV}^3$
A0	1.97	0.0	9.01×10^{-4}	0.0
JH	1.62	1.71×10^{-2}	2.83×10^{-4}	0.0
KMR	1.58	8.35×10^{-3}	2.32×10^{-4}	0.0
[11]	1.32	3.04×10^{-2}	1.68×10^{-3}	-9.08×10^{-3}
[15]	1.16	9.7×10^{-2}	-4.6×10^{-3}	-2.14×10^{-2}

FIG. 1.   The transverse momentum distribution of prompt J/ψ meson production in pp collisions at $\sqrt{s} = 7$ TeV. Left panel: the dashed, dotted, and dash-dotted curves correspond to the color-singlet $^3S_1^{(1)}$ and color-octet $^1S_0^{(8)}$ and $^3S_1^{(8)}$ contributions calculated with the KMR gluon density. The short dashed and short dash-dotted curves represent the feed-down contributions from the radiative decays of χ_c and $\psi(2S)$ mesons. The solid curve represent the sum of all these terms. Right panel: the solid, dashed, and dash-dotted curves correspond to the predictions obtained with the A0, JH, and KMR gluon distributions, respectively. The experimental data are from CMS [24].

eliminate visible disagreement. In the forward rapidity region, covered by the LHCb experiment, the difference between the predictions obtained with the different TMD gluon densities becomes more clear (see Fig. 3). The best description of LHCb data for $\sqrt{s} = 8$ TeV is provided by the A0 gluon distribution. The similar agreement of our predictions and the LHCb data is achieved for $\sqrt{s} = 7$ TeV (not shown). However, this gluon density is unable to describe LHCb data at $\sqrt{s} = 13$ TeV, that spoils the belief in the universality of the fitted NMEs. The JH'2013 gluon significantly overestimates these data at low $p_T < 6$ GeV and practically coincides with A0 predictions at larger transverse momenta. Therefore, we conclude that, similarly to the collinear factorization, including the low p_T data into the fitting procedure in the k_T-factorization approach can change the relative weight of different NMEs. However, as it was already mentioned above, the applicability of the NRQCD formulas at low transverse momenta is questionable. The results of calculations obtained with KMR gluon density are similar to the A0 ones at $y < 3$ and tend to overestimate the data at more forward rapidities, though still agree with the data within the uncertainties.

The ratios of the $\psi(2S)$ to J/ψ differential cross sections were measured by CMS Collaboration at $|y| < 1.2$ and $\sqrt{s} = 7$ TeV [24] and by ATLAS Collaboration at $\sqrt{s} = 7$ and 8 TeV in several rapidity subdivisions [23]. Additionally, the ratio $R_{13/8}$ of the double differential J/ψ production cross sections at $\sqrt{s} = 13$ TeV and $\sqrt{s} = 8$ TeV was presented by LHCb Collaboration [26]. Many of the experimental and theoretical uncertainties (as connected, for example, with the NMEs or hard scales) cancel out in these ratios, giving us possibility to further test

the production dynamics. Our predictions are shown in Figs. 4 and 5 and compared to the data. The cross sections of $\psi(2S)$ production are calculated in the same way as in our previous paper [5]. One can see that at low and moderate transverse momenta the $\psi(2S)$ to J/ψ production ratios are reasonably described by the considered TMD gluon densities everywhere except two last rapidity subintervals. The high p_T data (to be precise, at $p_T \geq 20$ GeV) can be used to discriminate between the TMD gluons. The difference becomes even more pronounced in the $R_{13/8}$ ratio (see Fig. 5).

Now we turn to the polarization of J/ψ mesons, which is the most interesting part of our study. In general, the spin density matrix of a vector particle decaying into a lepton pair depends on three angular parameters λ_θ, λ_ϕ, and $\lambda_{\theta\phi}$ which can be measured experimentally. The double differential angular distribution of the decay leptons can be written as [46]:

$$\frac{d\sigma}{d\cos\theta^* d\phi^*} \sim 1 + \lambda_\theta \cos^2\theta^* + \lambda_\phi \sin^2\theta^* \cos 2\phi^* + \lambda_{\theta\phi} \sin 2\theta^* \cos\phi^*, \qquad (14)$$

where θ^* and ϕ^* are the polar and azimuthal angles of the decay lepton measured in the J/ψ rest frame. The case of $(\lambda_\theta, \lambda_\phi, \lambda_{\theta\phi}) = (0, 0, 0)$ corresponds to unpolarized state, while $(\lambda_\theta, \lambda_\phi, \lambda_{\theta\phi}) = (1, 0, 0)$ and $(\lambda_\theta, \lambda_\phi, \lambda_{\theta\phi}) = (-1, 0, 0)$ refer to fully transverse and fully longitudinal polarizations. CMS [21] and LHCb [20] Collaborations have measured these parameters as functions of J/ψ transverse momentum in two complementary frames: the Collins-Soper and helicity ones. In addition, CMS Collaboration provided
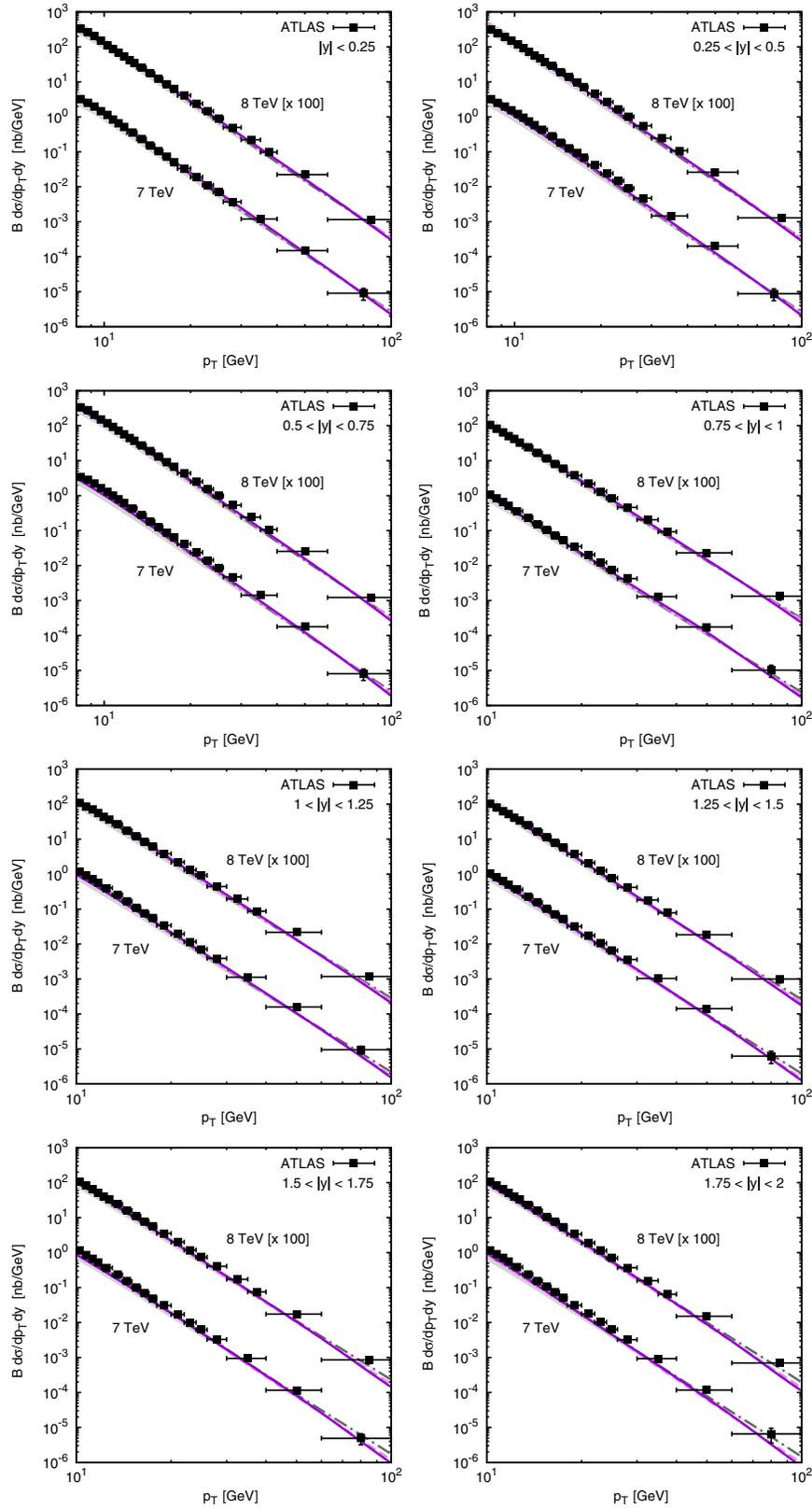
FIG. 2. The double differential cross sections of prompt J/ψ meson production in pp collisions at $\sqrt{s} = 7$ and 8 TeV. The solid, dashed, and dash-dotted curves correspond to the predictions obtained with the A0, JH, and KMR gluon densities, respectively. The shaded bands represent the usual scale variations in the KMR predictions, as it is described in the text. The experimental data are from ATLAS [23].
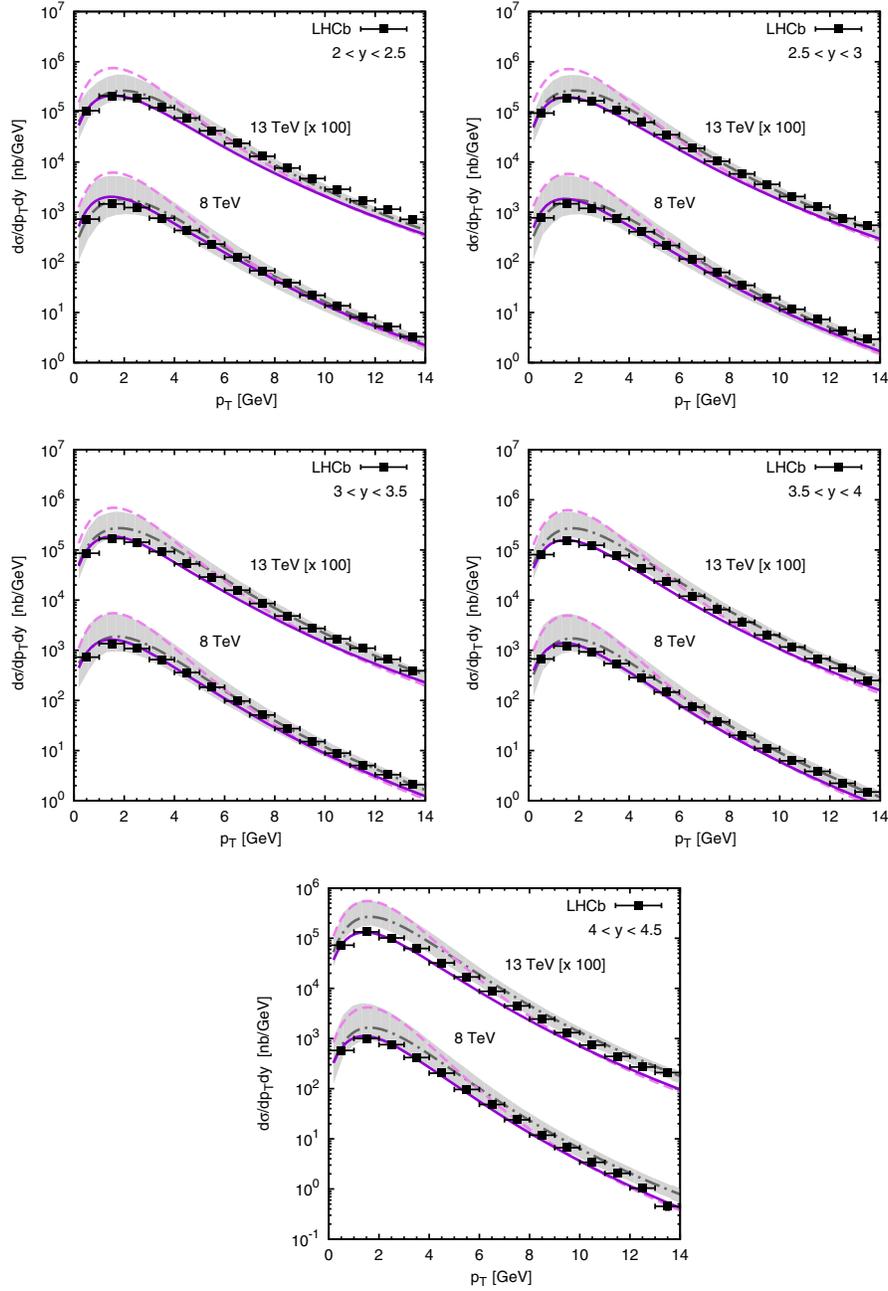
FIG. 3.   The double differential cross sections of prompt J/ψ meson production in pp collisions at $\sqrt{s} = 8$ TeV. Notation of all curves is the same as in Fig. 2. The experimental data are from LHCb [25].

measurements in the perpendicular helicity frame. In the Collins-Soper frame the polarization axis z bisects the two beam directions whereas the polarization axis in the helicity frame coincides with the direction of J/ψ momentum in the laboratory frame. In the perpendicular helicity frame the z axis is orthogonal to that in the Collins-Soper frame and lies in the plane spanned by the two beam momenta. Additionally, the frame-independent polarization parameter [21] $\lambda^* = (\lambda_\theta + 3\lambda_\phi)/(1 - \lambda_\phi)$ was investigated. Below we estimate the polarization parameters λ_θ, λ_ϕ, $\lambda_{\theta\phi}$, and λ^* for the CMS and LHCb conditions. Our calculation generally

follows the experimental procedure. We collect the simulated events in the kinematical region defined by the CMS and LHCb experiments, generate the decay lepton angular distributions according to the production and decay matrix elements, and then apply a three-parametric fit based on (14).

In Figs. 6–10 we confront our predictions for parameters λ_θ, λ_ϕ, $\lambda_{\theta\phi}$, and λ^* with the latest CMS [20] and LHCb [21] data. We find practically zero polarization ($\lambda_\theta \sim 0$) of the produced J/ψ mesons at moderate and large transverse momenta $p_T \geq 20$ GeV (see Figs. 6–8)
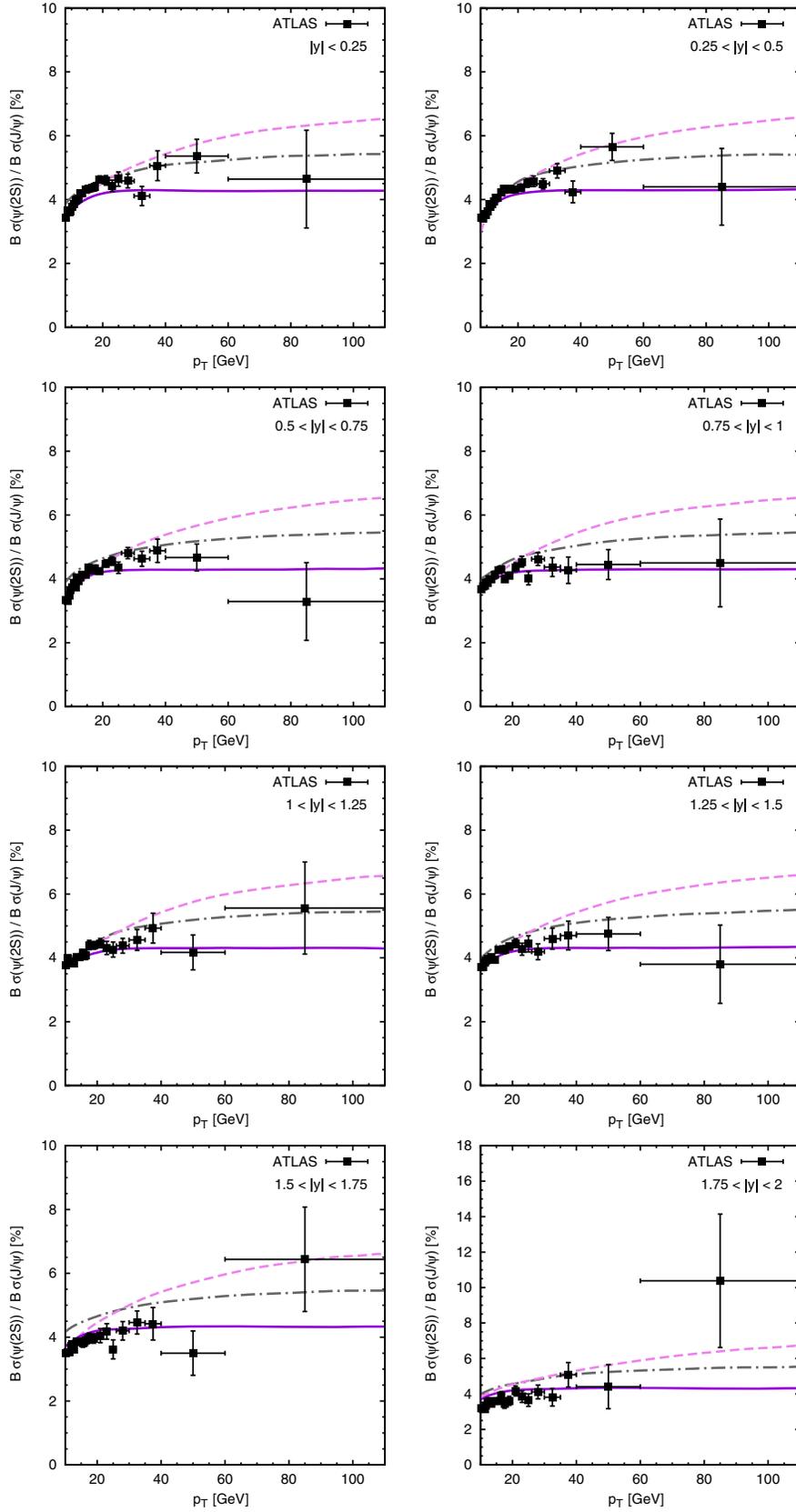
FIG. 4. Relative production rate $\sigma(\psi')/\sigma(J/\psi)$ calculated as a function of J/ψ meson transverse momenta at $\sqrt{s} = 8$ TeV. Notation of all curves is the same as in Fig. 2. The experimental data are from ATLAS [23].

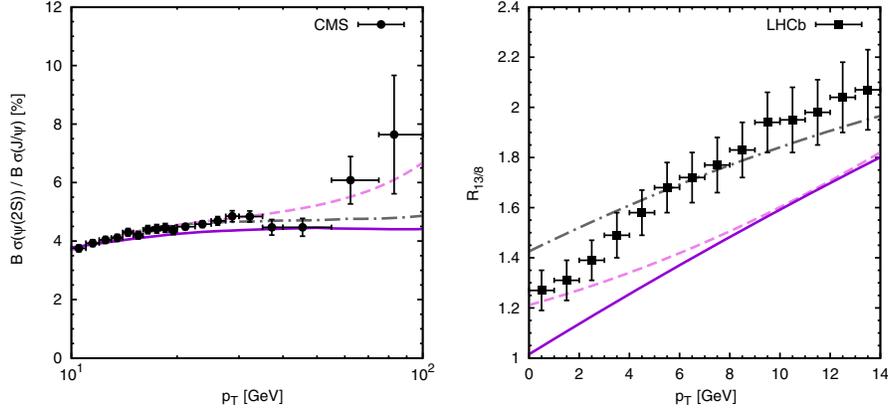FIG. 5.   Left panel: relative production rate $\sigma(\psi')/\sigma(J/\psi)$ calculated as a function of J/ψ meson transverse momenta at $\sqrt{s} = 7$ TeV. Right panel: relative ratio $R_{13/8}$ of the J/ψ meson production cross sections calculated at $\sqrt{s} = 13$ TeV and $\sqrt{s} = 8$ TeV. Notation of all curves is the same as in Fig. 2. The experimental data are from CMS [24] and LHCb [26].

and weak longitudinal polarization at low transverse momenta $p_T \leq 14$ GeV covered by the LHCb experiment. To be precise, we obtained $\lambda_\theta \sim 0.1$ in the Collins-Soper frame and $\lambda_\theta \sim -0.2$ in the helicity frame, respectively. Moreover, these results are practically independent of the J/ψ rapidity. As it was mentioned above, the traditional

NLO CS calculations predict large longitudinal polarization at high p_T, while the NRQCD predicts large transverse polarization, and none of these predictions is supported by experimental results. As one can see, treating the soft gluon emission within the NRQCD as a series of explicit color-electric dipole transitions [22] leads to unpolarized J/ψ
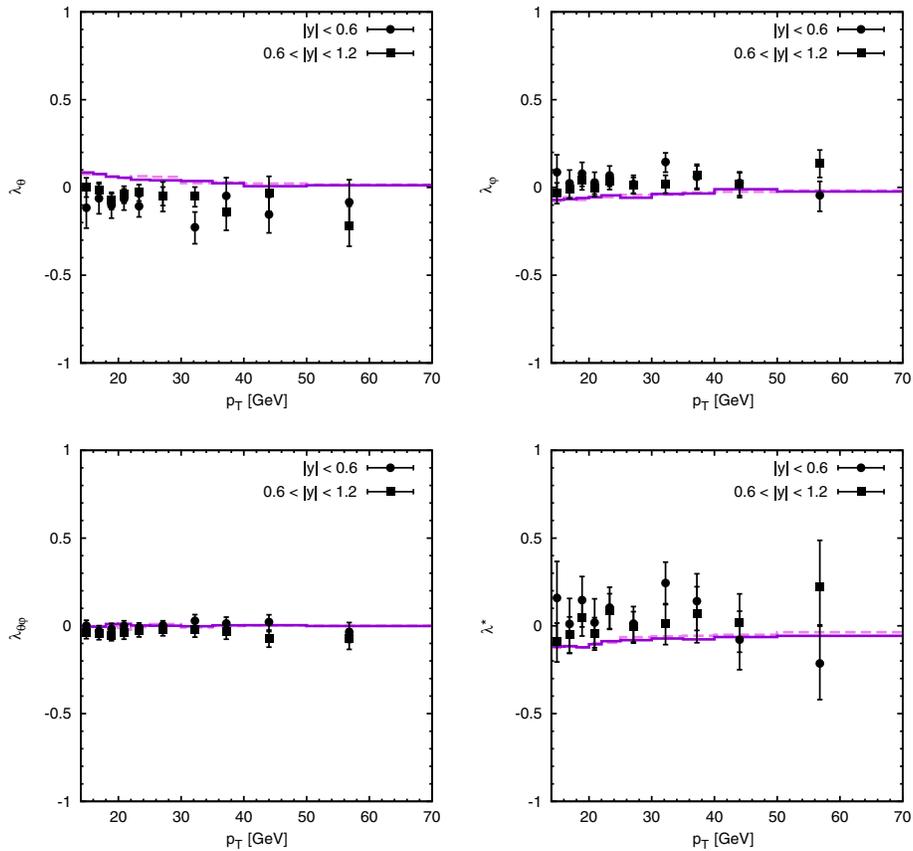

FIG. 6.   Polarization parameters λ_θ, λ_ϕ, $\lambda_{\theta\phi}$, and λ^* of prompt J/ψ mesons calculated as a function of their transverse momentum in the Collins-Soper frame. The solid and dashed histograms correspond to the predictions obtained at $|y| < 0.6$ and $0.6 < |y| < 1.2$, respectively. The KMR gluon distribution is used. The experimental data are from CMS [21].
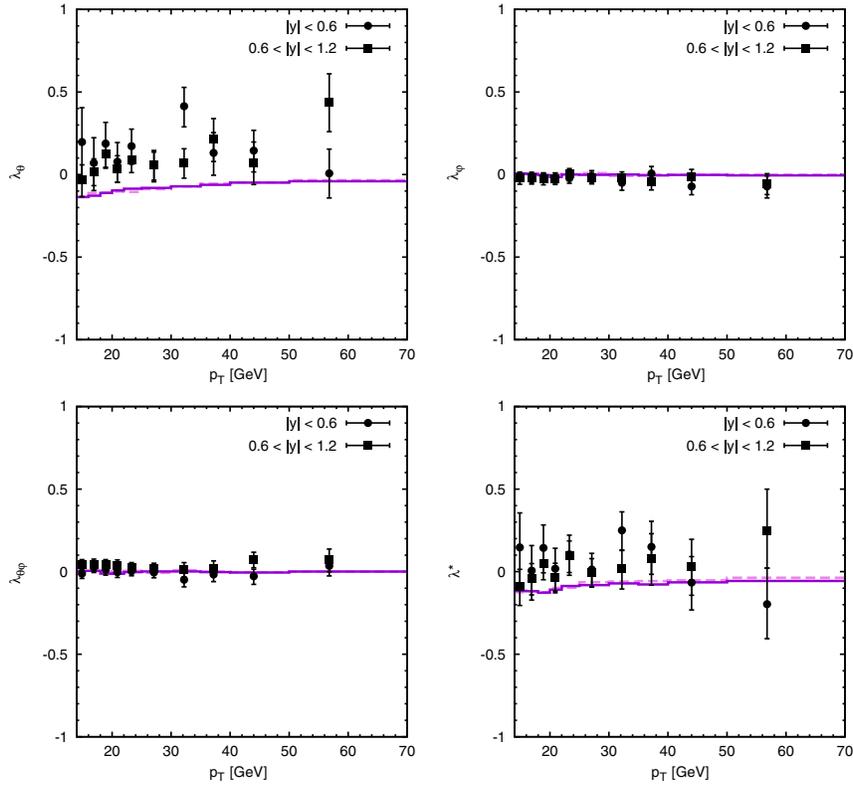
FIG. 7.   Polarization parameters $\lambda_\theta, \lambda_\phi, \lambda_{\theta\phi}$, and λ^* of prompt J/ψ mesons calculated as a function of their transverse momentum in the helicity frame. Notation of all curves is the same as in Fig. 6. The experimental data are from CMS [21].
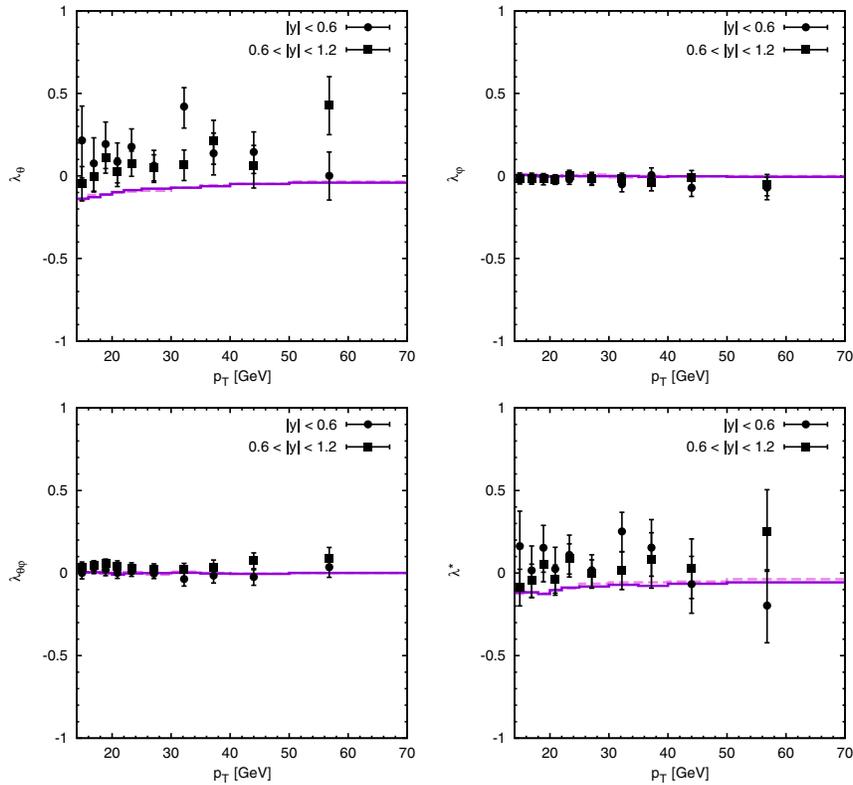

FIG. 8.   Polarization parameters $\lambda_\theta, \lambda_\phi, \lambda_{\theta\phi}$, and λ^* of prompt J/ψ mesons calculated as a function of their transverse momentum in the perpendicular helicity frame. Notation of all curves is the same as in Fig. 6. The experimental data are from CMS [21].
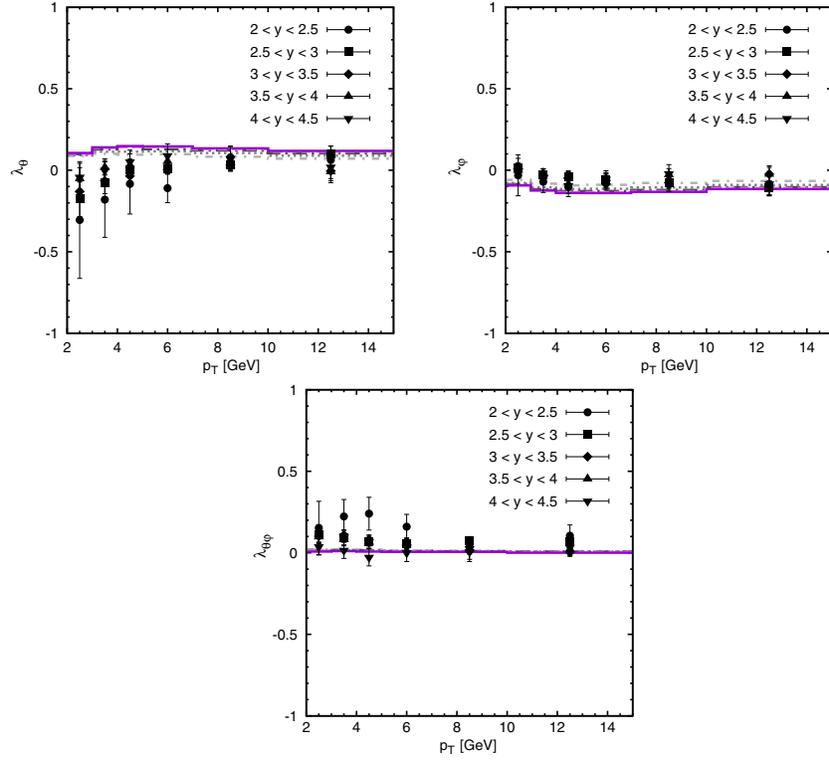
FIG. 9.   Polarization parameters λ_θ, λ_ϕ, and $\lambda_{\theta\phi}$ of prompt J/ψ mesons calculated as a function of their transverse momentum in the Collins-Soper frame. The solid, dashed, dash-dotted, dotted, and short dash-dotted histograms correspond to the predictions obtained at $2 < y < 2.5$, $2.5 < y < 3$, $3 < y < 3.5$, $3.5 < y < 4$, and $4 < y < 4.5$. The experimental data are from LHCb [20].
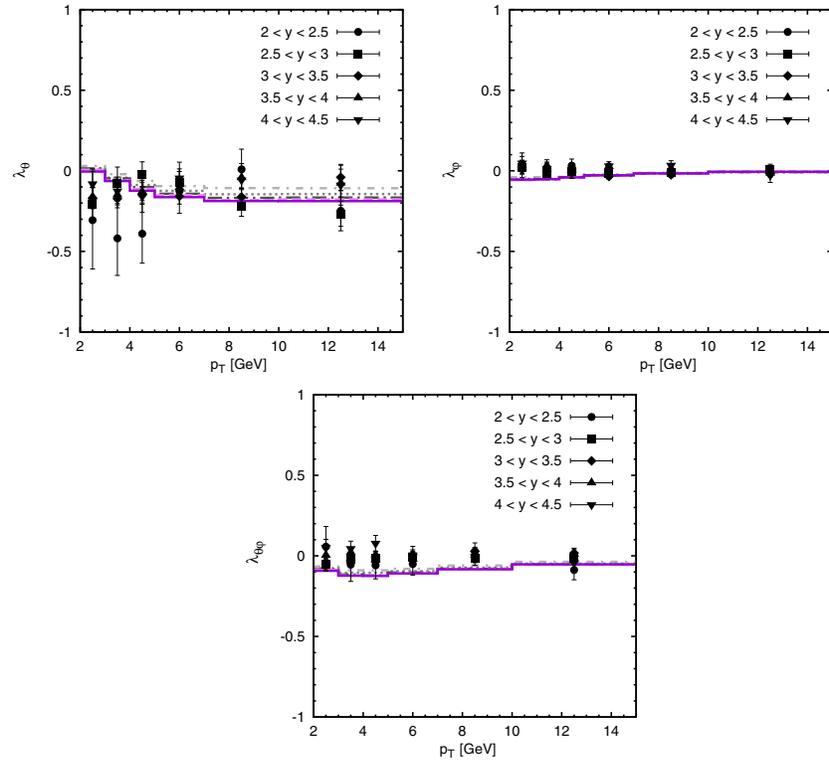

FIG. 10.   Polarization parameters λ_θ, λ_ϕ and $\lambda_{\theta\phi}$ of prompt J/ψ mesons calculated as a function of their transverse momentum in the helicity frame. Notation of all curves is the same as in Fig. 9. The experimental data are from LHCb [20].

production at high transverse momenta, that is in qualitative agreement with available LHC data. This remarkable property is the main result of our study, and the same conclusion was made previously in the case of prompt $\psi(2S)$ meson production [5]. Note that our interpretation of gluon radiation is not the same as in the conventional CS model at high-order pQCD, because the gluons are emitted by the entire $c\bar{c}$ system, not by individual quarks.

The absence of strong J/ψ polarization is not connected with parameter tuning, but seems to be a natural and rather general feature of the scenario [22]. We note, however, that while our predictions for λ_ϕ and $\lambda_{\theta\phi}$ parameters agree with the data, the description of λ_θ and λ^* is still rather qualitative than quantitative. Despite the huge experimental uncertainties, it could be due to the significant theoretical uncertainties connected, in particular, with the inclusion of NLO subprocesses and precise definition of NMEs. The detailed study of these uncertainties is out of our present paper. Nevertheless, the proposed way, in our opinion, can provide an easy and natural solution to a long-standing quarkonia polarization puzzle.

IV. CONCLUSIONS

We have considered prompt J/ψ production and polarization in pp collisions at the LHC in the framework of k_T-factorization approach. We have used the LO non-relativistic QCD formalism including both color-singlet and color-octet contributions and took into account both the direct production mechanism and the feed-down

contributions from χ_{c1}, χ_{c2}, and $\psi(2S)$ decays. Using the TMD gluon densities in a proton derived from the CCFM equation and from the Kimber-Martin-Ryskin prescription, we extracted the color-octet NMEs $\langle\mathcal{O}^\psi[^1S_0^{(8)}]\rangle$, $\langle\mathcal{O}^\psi[^3S_1^{(8)}]\rangle$, and $\langle\mathcal{O}^\psi[^3P_0^{(8)}]\rangle$ for J/ψ mesons from fits to transverse momentum distributions provided by the latest CMS measurements at $\sqrt{s} = 7$ TeV. Using the fitted NMEs, we have analyzed the data taken by the ATLAS, CMS, and LHCb Collaborations at different energies $\sqrt{s} = 7$, 8, and 13 TeV. We demonstrated the sensitivity of the different production rates, in particular, the ratios of the cross sections calculated at different energies, to the TMD gluon densities in a proton. We estimated the polarization parameters λ_θ, λ_ϕ, and $\lambda_{\theta\phi}$ which determine the J/ψ spin density matrix and demonstrated that treating the soft gluon emission as a series of explicit color-electric dipole transitions within the NRQCD leads to unpolarized J/ψ production at high transverse momenta, that is in qualitative agreement with the LHC data.

ACKNOWLEDGMENTS

[1] C. Chao-Hsi, Nucl. Phys. **B172**, 425 (1980); E. L. Berger and D. L. Jones, Phys. Rev. D **23**, 1521 (1981); R. Baier and R. Rückl, Phys. Lett. B **102**, 364 (1981); S. S. Gershtein, A. K. Likhoded, and S. R. Slabospitsky, Sov. J. Nucl. Phys. **34**, 128 (1981).

[2] E. Braaten and S. Fleming, Phys. Rev. Lett. **74**, 3327 (1995).

[3] G. Bodwin, E. Braaten, and G. Lepage, Phys. Rev. D **51**, 1125 (1995).

[4] P. Cho and A. K. Leibovich, Phys. Rev. D **53**, 150 (1996); Phys. Rev. D **53**, 6203 (1996).

[5] S. P. Baranov, A. V. Lipatov, and N. P. Zotov, Eur. Phys. J. C **75**, 455 (2015).

[6] S. P. Baranov, A. V. Lipatov, and N. P. Zotov, Phys. Rev. D **93**, 094012 (2016).

[7] P. Artoisenet, J. Campbell, J. P. Lansberg, F. Maltoni, and F. Tramontano, Phys. Rev. Lett. **101**, 152001 (2008).

[8] J. P. Lansberg, Phys. Lett. B **695**, 149 (2011).

[9] ATLAS Collaboration, J. High Energy Phys. 09 (2014) 079.

[10] M. Butenschön and B. A. Kniehl, Phys. Rev. D **84**, 051501 (2011).

[11] M. Butenschön and B. A. Kniehl, Phys. Rev. Lett. **106**, 022003 (2011).

[12] Y.-Q. Ma, K. Wang, and K. T Chao, Phys. Rev. Lett. **106**, 042002 (2011).

[13] M. Butenschön and B. A. Kniehl, Phys. Rev. Lett. **108**, 172002 (2012).

[14] K.-T. Chao, Y.-Q. Ma, H.-S. Shao, K. Wang, and Y.-J. Zhang, Phys. Rev. Lett. **108**, 242004 (2012).

[15] B. Gong, L.-P. Wan, J.-X. Wang, and H.-F. Zhang, Phys. Rev. Lett. **110**, 042002 (2013).

[16] P. Faccioli, V. Knuenz, C. Lourenco, J. Seixas, and H. K. Woehri, Phys. Lett. B **736**, 98 (2014).

[17] CDF Collaboration, Phys. Rev. Lett. **99**, 132001 (2007).

[18] CDF Collaboration, Phys. Rev. Lett. **108**, 151802 (2012).

[19] LHCb Collaboration, Eur. Phys. J. C **74**, 2872 (2014).

[20] LHCb Collaboration, Eur. Phys. J. C **73**, 2631 (2013).

[21] CMS Collaboration, Phys. Lett. B **727**, 381 (2013).

[22] S. P. Baranov, Phys. Rev. D **93**, 054037 (2016).

[23] ATLAS Collaboration, Eur. Phys. J. C **76**, 1 (2016).

[24] CMS Collaboration, Phys. Rev. Lett. **114**, 191802 (2015).

[25] LHCb Collaboration, J. High Energy Phys. 06 (2013) 064.

[26] LHCb Collaboration, J. High Energy Phys. 10 (2015) 172.

[27] L. V. Gribov, E. M. Levin, and M. G. Ryskin, Phys. Rep. **100**, 1 (1983); E. M. Levin, M. G. Ryskin, Yu. M. Shabelsky, and A. G. Shuvaev, Sov. J. Nucl. Phys. **53**, 657 (1991).

[28] S. Catani, M. Ciafaloni, and F. Hautmann, Nucl. Phys. **B366**, 135 (1991); J. C. Collins and R. K. Ellis, Nucl. Phys. **B360**, 3 (1991).

[29] E. A. Kuraev, L. N. Lipatov, and V. S. Fadin, Sov. Phys. JETP **44**, 443 (1976); **45**, 199 (1977); I. I. Balitsky and L. N. Lipatov, Sov. J. Nucl. Phys. **28**, 822 (1978).

[30] M. Ciafaloni, Nucl. Phys. **B296**, 49 (1988); S. Catani, F. Fiorani, and G. Marchesini, Phys. Lett. B **234**, 339 (1990); Nucl. Phys. **B336**, 18 (1990); G. Marchesini, Nucl. Phys. **B445**, 49 (1995).

[31] B. Andersson *et al.* (Small-*x* Collaboration), Eur. Phys. J. C **25**, 77 (2002); J. Andersen *et al.* (Small-*x* Collaboration), Eur. Phys. J. C **35**, 67 (2004); **48**, 53 (2006).

[32] B. A. Kniehl, D. V. Vasin, and V. A. Saleev, Phys. Rev. D **73**, 074022 (2006).

[33] S. P. Baranov, Phys. Rev. D **91**, 034011 (2015).

[34] P. Cho, M. Wise, and S. Trivedi, Phys. Rev. D **51**, R2039 (1995).

[35] E. Bycling and K. Kajantie, *Particle Kinematics* (John Wiley and Sons, New York, 1973).

[36] S. P. Baranov and A. Szczurek, Phys. Rev. D **77**, 054016 (2008).

[37] G. P. Lepage, J. Comput. Phys. **27**, 192 (1978).

[38] H. Jung, arXiv:hep-ph/0411287.

[39] F. Hautmann and H. Jung, Nucl. Phys. **B883**, 1 (2014).

[40] M. A. Kimber, A. D. Martin, and M. G. Ryskin, Phys. Rev. D **63**, 114027 (2001); G. Watt, A. D. Martin, and M. G. Ryskin, Eur. Phys. J. C **31**, 73 (2003).

[41] A. D. Martin, W. J. Stirling, R. S. Thorne, and G. Watt, Eur. Phys. J. C **63**, 189 (2009).

[42] PDG Collaboration, Chin. Phys. C **38**, 090001 (2014).

[43] Ph. Hägler, R. Kirschner, A. Shäfer, L. Szymanowski, and O. V. Teryaev, Phys. Rev. D **63**, 077501 (2001).

[44] F. Yan and K. T. Chao, Phys. Rev. Lett. **87**, 022002 (2001).

[45] S. P. Baranov, A. V. Lipatov, and N. P. Zotov, Phys. Rev. D **85**, 014034 (2012).

[46] M. Beneke, M. Krämer, and M. Vänttinen, Phys. Rev. D **57**, 4258 (1998).